The Astrophysical Journal, 581:610–625, 2002 December 10

THE EFFECTIVE TEMPERATURES OF MID-O STARS[1]

Luciana Bianchi[2] and Miriam Garcia[2,3]
Received 2002 June 6; accepted 2002 August 12

ABSTRACT

We derived photospheric parameters, mass-loss rates, and wind velocities of Galactic O6–O7 stars by analyzing high-resolution spectra in the far-UV and UV ranges with line-blanketed, hydrodynamic, non-LTE spherical models. We combined spectra from the *Far Ultraviolet Spectroscopic Explorer* (*FUSE*) in the range 905–1187 Å and *International Ultraviolet Explorer* (*IUE*) archival spectra (1150–3250 Å) and used the WM-BASIC code of Pauldrach et al. to compute model spectra. Lines in the *FUSE* range include high ionization stages (e.g., O VI) and lower abundance non-CNO elements (e.g., P V). Analyzed in addition to the N IV, N V, Si IV, and C IV lines in the *IUE* range, these features play a crucial role in uniquely constraining the stellar parameters, assessing the presence of shocks in the wind, and quantifying the effects of the resulting soft X-rays on the wind ionization. The effective temperatures derived from the consistent analysis of the far-UV and UV spectra are significantly (≈6000 K or 15% on average, or between 4000 and 8000 K) lower than most values previously derived for some of our targets and lower than typical values assigned to their spectral types from different compilations. This result has great implications for our understanding of the evolution of massive stars and the characterization of young stellar populations, as well as for energy balance calculations of H II regions.

Subject headings: stars: early-type — stars: fundamental parameters — stars: mass loss — stars: winds, outflows — ultraviolet: stars

On-line material: color figures

1. INTRODUCTION

Hot massive stars play a primary role in the chemical evolution of the universe, because of the rapid and effective production of heavy elements during their fast life cycles. They also play a crucial role in the ionization of H II regions and in the dynamics of the interstellar medium (ISM), by sculpting vast bubbles through their highly supersonic stellar winds and intense UV radiation, thus influencing the physical conditions of the ISM and star formation. Compared to the more easily characterized lower mass portions of the H-R diagram, accurate measurements of the high-mass end of the initial mass function (IMF) in stellar populations and of the stellar parameters of massive stars are elusive for several reasons: massive stars are rare, they evolve rapidly, and photometric data at optical wavelengths are rather insensitive to their hot temperatures (e.g., Bianchi et al. 2001; Massey 1998 for a review), making their global characterization uncertain without detailed spectroscopy. Even when adequate spectroscopic data are available, modeling is complicated by the non-LTE conditions and by the wind hydrodynamics (mass loss and acceleration) and sphericity effects, all nonnegligible. The supersonic winds of hot stars are revealed by conspicuous P Cygni profiles of transitions that are found, for the most abundant ionic species in the wind, below 2000 Å. The wavelength region accessible to *International Ultraviolet Explorer* (*IUE*) and *Hubble Space Telescope* (*HST*; longward of 1150 Å) contains strong resonance lines of C IV, N V, and Si IV. These lines give useful information on the wind terminal velocity but are often saturated and alone are not sufficient to determine the mass-loss rate and the ionization structure of the wind. The 905–1187 Å range covered by the *Far Ultraviolet Spectroscopic Explorer* (*FUSE*) satellite (Moos et al. 2000) includes a greater spread of species and ionization states, and non-CNO elements (e.g., Bianchi et al. 2000; Pellerin et al. 2002; Walborn et al. 2002). These transitions allow for the first time since *Copernicus* a consistent analysis of several ionic species sampling different depths in the envelope, to solve the wind ionization structure and therefore to measure mass-loss rates and physical conditions in the expanding envelopes. An alternative reliable method to determine mass-loss rates has been the analysis of the Hα profile, since the hydrogen ionization does not suffer from uncertainties (e.g., Bianchi et al. 1994; Scuderi & Panagia 1992; Puls et al. 1996); however, this line samples only the conditions in the deepest layers and gives limited information on the outer envelope.

We present first results from a comprehensive program aimed to analyze (by consistent modeling) high-resolution spectra from the optical regime to the far-UV of hot stars covering different spectral types and luminosity classes. This paper explores the properties of mid-O Galactic stars of different luminosity classes. In § 2 details about the observations used and about the program stars are given. Section 3 contains a comparative analysis of the spectral morphology among the sample, and § 4 describes the derivation of stellar parameters via synthetic spectral modeling. In § 5 the implications of our findings are discussed.

[1] Based on observations with the NASA-CNES-CSA *Far Ultraviolet Spectroscopic Explorer*, which is operated by The Johns Hopkins University under NASA contract NAS5-32985, and on *IUE* observations from the MAST and INES archives.

[2] Center for Astrophysical Sciences, The Johns Hopkins University, Department of Physics and Astronomy, 239 Bloomberg Center for Physics and Astronomy, 3400 North Charles Street, Baltimore, MD 21218; bianchi@pha.jhu.edu, garcia@pha.jhu.edu.

[3] University of La Laguna, Department of Astrophysics, Tenerife, Spain.

TABLE 1
PROGRAM STARS AND DATA SETS

Star	Sp. Type[a] [Ref.]	V	LSR Velocity [Ref.] (km s^{-1})	log L_X (ergs s^{-1})	*FUSE* Data Sets	*IUE* Data Sets
HD 163758.....	**O6.5 Iaf** [1, 2]; O6f [3]; O7 If [4]	7.32	−48 [5]	...	P1015901	SWP02892
HD 192639.....	**O7 Ib(f)** [6]; O7.5 IIIf [7]	7.11	−6 [8]	...	P1162401	SWP09493
HD 210839 (λ Cep)	**O6f II** [9]; O6 I(n)fp [10]; O6ef [7]	5.1	−75.9 [11]	32.19 ± 0.32,[b,c] 31.81[c,d]	P1163101	SWP52623
HD 157857.....	**O6.5 III(f)** [6]; O7(f) [7]	7.78	+59 [8]	<32.76[b]	P1027501	SWP10026
HD 93843	**O5–6 III(f)** [10]; O6 III(f) [6]	7.33	−9.9 [11]	33.07 ± 0.30[b]	P1024001	SWP07723
HD 101298.....	**O6 V** [10]; O6 V((f)) [1]	8.16	−0.7 [11]	32.58 ± 0.30[b]	P1025201	SWP06939

[a] The spectral types adopted in this work are given in boldface.
[b] Measurements from *Einstein* satellite in the 0.2–3.5 KeV range (Chlebowski, Harnden, & Sciortino 1989).
[c] For HD 210839, L_X has been rescaled to the *Hipparcos* distance of 0.5 kpc (Perryman et al. 1997), since the distance used by Chlebowski et al. 1989 and Berghoefer, Schmidtt, & Cassinelli 1996 (0.8 kpc in both papers) is very different.
[d] Measurements from the *ROSAT* satellite in the 0.1–2.4 keV energy band (Berghoefer et al. 1996).

REFERENCES.—(1) Walborn & Panek 1984; (2) Garrison, Hiltner, & Schild 1977; (3) McConnell & Bidelman 1976; (4) Leep 1978; (5) Thackeray, Tritton, & Walker 1973; (6) Walborn 1972; (7) Conti & Leep 1974; (8) Evans 1967; (9) this paper; (10) Walborn 1973; (11) Conti, Leep, & Lorre 1977.

2. THE PROGRAM STARS AND THE OBSERVATIONS

2.1. *Data and Reduction*

Table 1 lists relevant information on the program stars compiled from the literature and the data used in our analysis. The *FUSE* data were taken in the $30'' \times 30''$ (LWRS) aperture. The data were reprocessed with the pipeline CalFUSE, version 2.0.5, which provides a major improvement in the spectral extraction, background subtraction, and wavelength calibration.[4] Individual segments from all SiC and LiF channels were examined in the two-dimensional reconstructed spectra, to check against data defects such as event bursts or the "worm" (Sahnow et al. 2000) and to verify optimum centering of the extraction windows. The segments of the extracted spectra were then checked to verify consistency of flux level and wavelength scale among the different channels, and finally, the good portions from all segments were combined to achieve the maximum possible signal-to-noise ratio. The *FUSE* spectral resolution ($R \approx 20,000$) exceeds the requirement for the analysis of broad stellar wind lines; however, it is essential to assess the presence of interstellar absorptions (mainly H I and H_2 transitions) that affect large parts of many stellar line profiles (see Fig. 1). For clarity, we rebinned the *FUSE* spectra with 0.25 Å bins in our figures. The *FUSE* data used in this analysis were taken by various GT *FUSE* Science Team programs for different science goals (studies of the ISM): P101 for HD 163758, P116 for HD 210839 and HD 192639, and P102 for HD 93843, HD 101298, and HD 157857.

In the UV range, we used *IUE* high-resolution ($\approx$0.2 Å) data taken from the Multimission Archive at the Space Telescope Science Institute (MAST) and the *IUE* Newly Extracted Spectra (INES) archive (Wamsteker et al. 2000). We used MAST for a quick detailed examination and comparison of the available data, to chose the best data sets. Two slightly different processings for the *IUE* high-resolution data are used by MAST and INES. The order overlap correction in the echelle *IUE* spectra affects severely the depth of the N V absorption (see Bianchi & Bohlin 1984), and we eventually used the reprocessed spectra from INES, which provide a better background correction for our cases.

2.2. *The Program Stars*

Spectral classification of hot stars is somewhat complex, because of wind and metallicity effects; variability and peculiarities are not uncommon. Therefore, we took great care in selecting as "bona fide" as possible objects representative of mid-O spectral types, covering different luminosity classes. In Table 1 and in the comments below we summarize relevant information from an exhaustive literature search, for the objects studied. Mason et al. (1998) performed speckle interferometry of a number of Galactic stars to check for binary systems. All of our program stars are included in their study, and none was found to be double with this technique.

HD 163758 was classified as O7 If by Leep (1978) and as O6.5 Iaf by Walborn (1973). Gómez & Niemela (1987) confirm, from optical spectroscopy, that the star is not a binary and that it has normal CNO abundances, although it appears an "Of" star. There is only one *IUE* high-dispersion spectrum in the short-wavelength region: a few pixels are saturated but not in the regions of interest.

For HD 210839 we chose the only *IUE* SWP high resolution spectrum that is not saturated. Optical spectral classifications concur to type O6 I(n)fp (Walborn 1973), O6 If (Mathys 1989), and O6ef (Conti & Leep 1974).

HD 157857 was classified as O6.5 III(f) by Walborn (1972) and by Mathys (1988) from its optical spectrum, and its UV (*IUE*) spectrum was found consistent with this type (O6.5 III; Penny, Gies, & Bagnuolo 1996). Of two high-resolution SWP spectra available in the *IUE* archive, we chose SWP10026, which has slightly better quality.

HD 93843 was found to be slightly variable in spectral subclass, between O6 and O5, but not in luminosity class, by Walborn (1973). Like most O-type stars, wind line profiles exhibit slight short-term variability, because of (unstable) inhomogeneities in the wind. A series of *IUE* spectra showed short-term line profile variability at 10% of the continuum level at most (Prinja & Crowther 1998), but the overall average line profiles repeat very well over the years (e.g., from 1980 to 1996, when *IUE* observing campaigns were repeated). We used a well-exposed *IUE* spectrum taken

[4] See V. Dixon, J. Kruk, & E. Murphy (2002), The CalFUSE Pipeline Reference Guide, available at http://fuse.pha.jhu.edu/analysis/pipeline_reference.html.

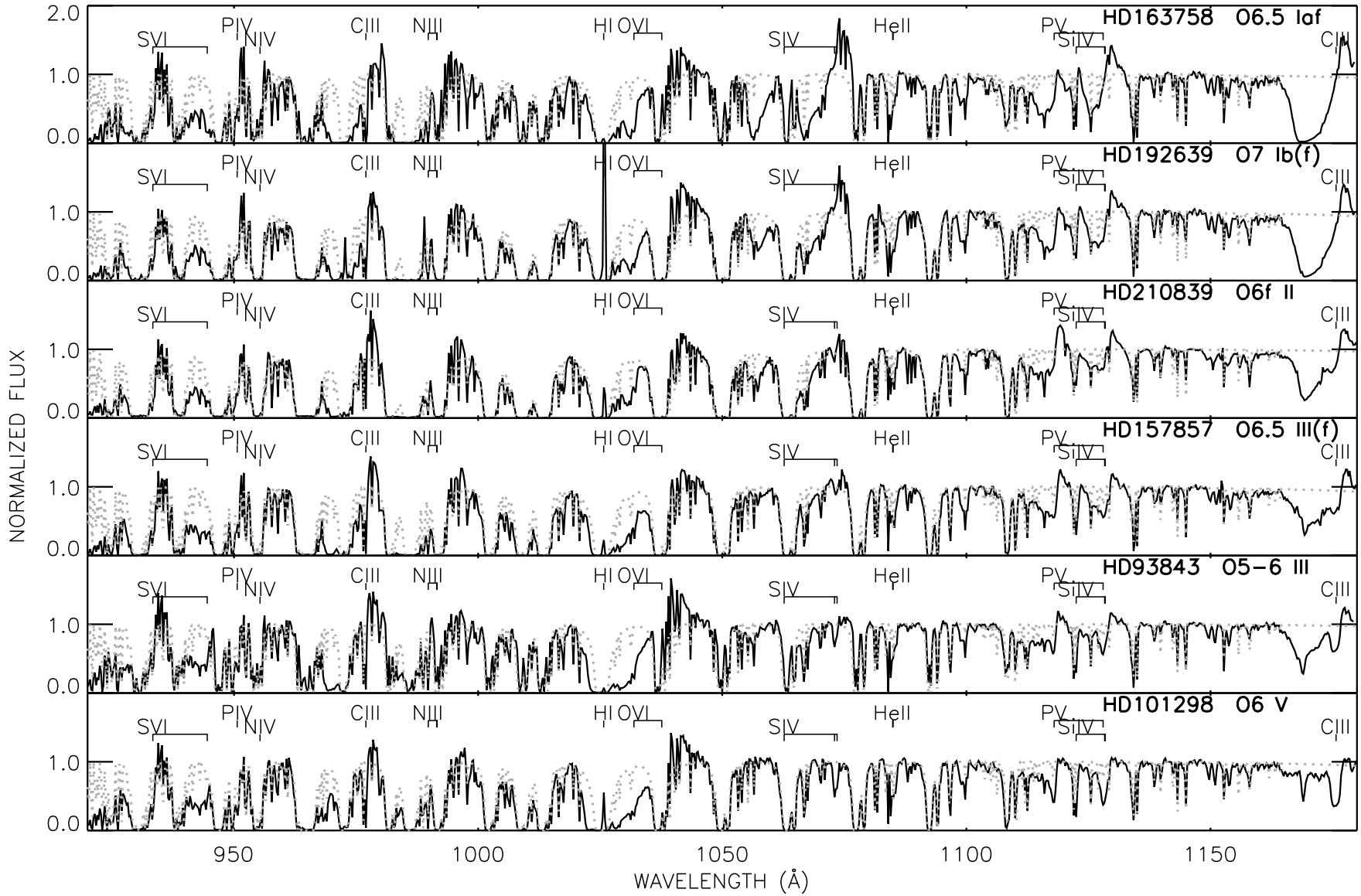

FIG. 1.—Sequence of spectra in the *FUSE* range (*black line*). To guide the eye to recognize the bona fide stellar features, we show models of H_2 plus H I absorptions (*dotted line*), calculated with column densities appropriate for each star's $E(B-V)$. The H_2 plus H I models help identify which parts of the stellar features are not affected by the ISM absorptions and therefore were given weight in the model fits. The H_2 plus H I models were also necessary to perform an accurate normalization of the flux to the continuum level. Very few regions in the spectra can be used for this purpose, and these can be identified only by examining the spectra and the ISM models concurrently. Note the O VI emission common to all stars and the dependence of C III λ1175 (plus C IV λ1169 becoming separated at low luminosity classes) and P V on luminosity. As shown by our model analysis, these features strongly depend on mass-loss rate. The red component of the S IV doublet (the shorter wavelength component is affected by a strong interstellar H_2 absorption band) varies from a fully developed P Cygni profile in the supergiants to a narrow absorption in the dwarf star. [*See the electronic edition of the Journal for a color version of this figure.*]

through the small (2″) aperture, which gives the maximum resolution. The absolute flux is lower than in spectra taken through the large (10″ × 20″) aperture, since the *IUE* small aperture transmits only about 50% of the flux; however, in the normalized spectra the line profiles are consistent among small and large aperture data.

HD 192639 was classified as O7 Ib(f) by Walborn (1972) from its optical spectrum, and the UV spectrum was found to be consistent with this type (Penny et al. 1996). There is only one *IUE* SWP high-resolution spectrum, of good quality except for some saturated pixels in the Si IV emission and longward of the region of interest.

HD 101298 was classified as O6 V type based on its optical spectrum by Walborn (1973). This classification was confirmed based on the morphology of its UV (*IUE*) spectrum by Walborn & Panek (1984). There is only one *IUE* SWP high-resolution spectrum available, of good quality.

3. ANALYSIS OF THE SPECTRAL MORPHOLOGY

The general trends of UV and far-UV line variations with spectral types have been discussed in several atlases, notably by Walborn, Nichols-Bohlin, & Panek (1985) and Walborn & Nichols-Bohlin (1987) in the *IUE* range and recently by Pellerin et al. (2002) in the *FUSE* range, for Milky Way stars, and by Walborn et al. (2002) for Magellanic Cloud stars. We begin our analysis with a detailed discussion of line variations among the luminosity classes spanned by our sample, in more depth and including also less prominent features than those described in the atlases. This discussion supports the following sections, where we explain the observed variations in terms of physical parameter changes, by quantitative modeling of the spectra.

The *FUSE* and *IUE* spectra of our program stars are shown in Figures 1 and 2, respectively, arranged in a sequence that produces a continuous variation of the line morphology across the sample and that will be confirmed by our modeling (§ 4) to be a sequence of decreasing stellar radii and luminosities. In the *FUSE* range (Fig. 1) we show also models of interstellar H_2 plus H I absorptions (*gray dotted line*), calculated with column densities inferred from each star's $E(B-V)$ using the relationships of Bohlin, Savage, & Drake (1978), except for HD 210839 and HD 192639, where we used accurate column densities derived by Rachford et al. (2002) from the analysis of *FUSE* spectra. We did not attempt to fit precisely the interstellar lines (which is beyond our purpose and is pursued by other authors): the H_2 plus H I models are shown only to identify which parts of the stellar features are not affected by the interstellar absorptions and therefore were given weight in the stellar model fits. This is relevant to the analysis in the following sections. The H_2 plus H I models were also necessary to perform an accurate normalization of the flux to the continuum. Very few regions in the spectra can be used for this purpose, and these can be identified only by examining the spectra and the ISM models concurrently. With a detailed examination, one can note (Fig. 1) that some spectral regions where there are no stellar lines are still absorbed by several hydrogen lines, and thus the actual continuum is lower than 1.0 (in the normalized spectra) and matches our ISM model. Thus, we believe we achieved the highest possible accuracy by performing the spectrum normalization concurrently with modeling of the ISM absorptions.

3.1. *The Supergiant Stars*

For HD 192639 and HD 163758, the *FUSE* spectra are basically identical except for S IV, which is significantly stronger in HD 163758 (both emission and absorption). C III λ1175 is also slightly stronger in HD 163758, although the effect is marginal because of uncertainty in the normalization, since this multiplet falls at the edge of the range in both the *FUSE* and *IUE* spectra. In the *IUE* range, Si IV and N V are stronger in HD 163758, while N IV, C IV, and several weaker lines (e.g., He II) are similar. The strength of Si IV increases with increasing mass-loss rate and decreasing temperature (as does S IV). Our consistent spectral modeling (next section) will confirm that the difference in line strength can be ascribed to these effects. The N V doublet depends strongly on $T_{\rm eff}$ (increasing with temperature), which, however, does not vary significantly within our sample, and heavily on the X-ray ionization caused by shocks. This line, together with O VI, primarily constrains the amount of shock-produced X-rays in the wind. The sensitivity of individual lines to other parameters will be discussed in more detail in § 4.

HD 210839, although classified of the same luminosity class as the two previous objects from its optical lines, exhibits a far-UV to UV spectrum different from the other two supergiants: C III λ1175 is significantly weaker, and Si IV and S IV are weaker in HD 210839. C IV λ1550 appears to have a slightly stronger emission. All these differences indicate a higher ionization, which may be ascribed to the earlier subtype of HD 210839 (O6, while the two supergiants discussed previously have types O6.5–O7). However, P V, C III, and Si IV also indicate lower mass-loss rates.

The high-ionization O VI doublet is strong in all three supergiants, although its emission slightly decreases from HD 192639 to HD 163758 to HD 210839. The P V doublet in HD 210839 has a stronger emission but a weaker absorption compared to both the other supergiants. The apparently stronger P V emission is probably due to a different relative strength of the nearby Si IV doublet. The lines of this doublet hardly affect the P Cygni profiles of the P V doublet in HD 210839, while they may be absorbing the red component, and the emission of the blue component of P V, in the other stars.

A few less conspicuous features are also worthy of discussion. Note in all three supergiants the absorption line near 1099 Å, of slightly decreasing strength from HD 192639 to HD 163758 to HD 210839. This line was also reported (as an unidentified feature) in late-O supergiants by Walborn & Bohlin (1996) in their *Copernicus* atlas of Galactic stars. By examining our extensive grid of theoretical models (§ 4), we find a very small absorption, due to an O IV λ1099.2 line, plus several lines of Fe III, Fe IV, Fe V, Ni IV, and Si III. Its strength is rather insensitive to the stellar parameters in our range, because the relative ratios of O IV to Si III (and of the other ions contributing to this small feature) vary with temperature within the blend. Additionally, we suspect it is partly of interstellar origin.

Another interesting feature that exhibits large variations among the three supergiants is the absorption at 1200 Å, very strong in HD 163758 and much weaker in the others. This feature is identified as a blend of primarily Si III with S III and S V (see § 4.5) and is partly interstellar. There is another S V line in the *IUE* range (λ1501.8), which is observed as a small absorption and predicted by the models;

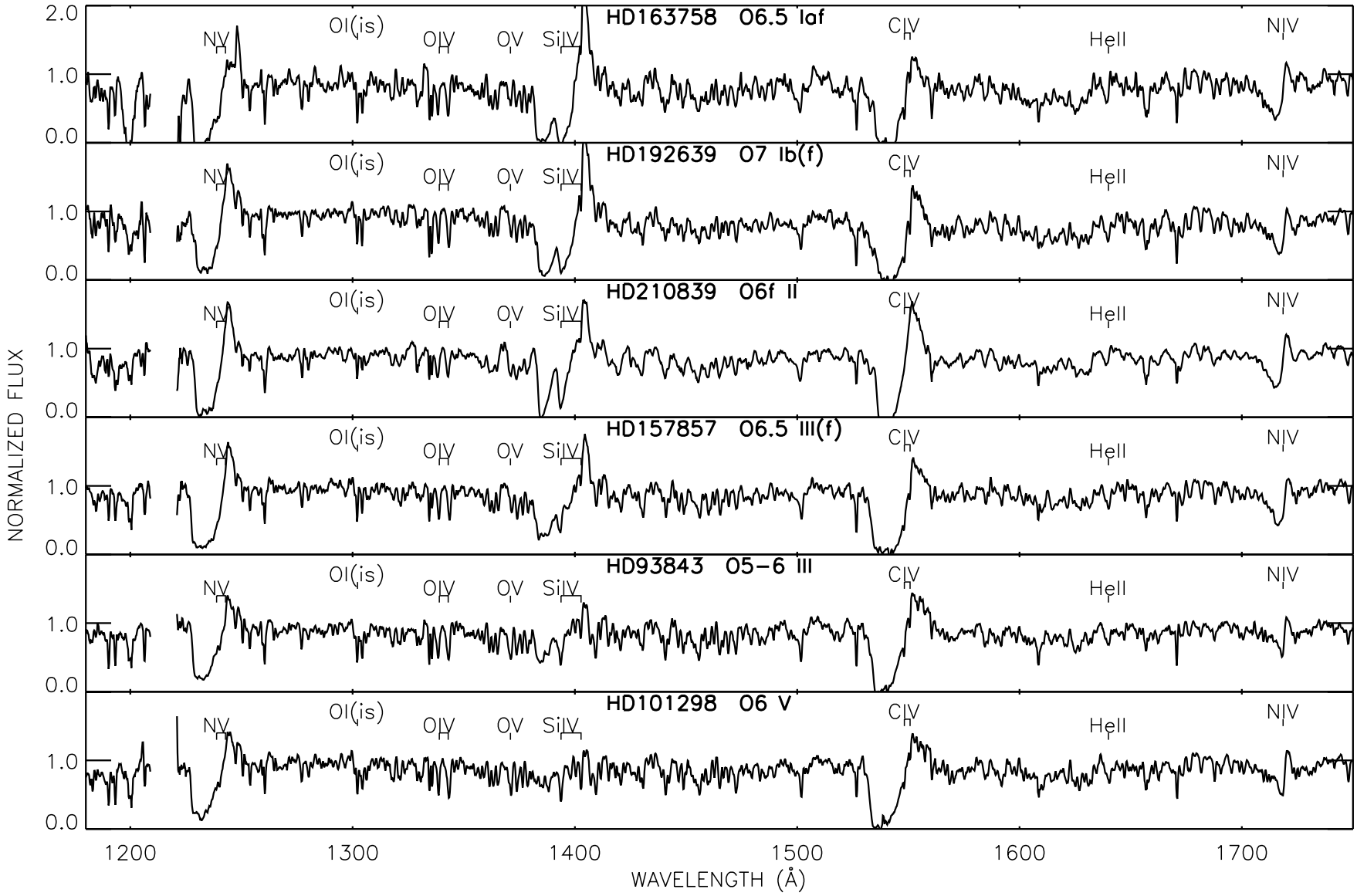

FIG. 2.—Sequence of spectra in *IUE* range. Here the strongest variation among luminosity classes is in the Si IV doublet, which is extremely sensitive to the mass-loss rate. The strong P Cygni profiles of C IV and N V are saturated in the supergiants and thus rather insensitive to mass-loss rate variations within a wide range; however, because they are fully developed profiles and not affected by interstellar absorptions, they are useful for determining precisely the terminal velocity. Note in this plot and in the previous figure that many lines exhibit a continuous variation across the sample, confirming our suggested reclassification of HD 210839 to class II.

however, it does not change among our sample. Consistently, from our model grid the line does not vary within the acceptable range of stellar parameters. These lines will be discussed again in § 4.5.

The resonance line of He II λ1640 is very weak at these later types and lies near a broad depression of the continuum due to blends of Fe II and Fe III (conspicuous at high luminosity classes), and no variations among the sample are appreciable.

3.2. *The Giant Stars*

The two giants of our sample exhibit very similar spectra in all features, with the exception of Si IV (stronger P Cygni in HD 157857) and O VI (weaker emission in HD 157857). One of the parameters affecting these lines in opposite ways is the amount of shocks: fewer shocks imply lower X-ray flux, thus lower ionization, which favors Si IV and decreases O VI. Our analysis (see later) will instead indicate that the effect is likely due to different mass-loss rates in this case. The effect is reported here to stress the importance of a consistent analysis of several lines for a unique interpretation and solution of the physical parameters. A less conspicuous difference is seen in the lines of N V λ1240 and N IV λ1720, slightly stronger in HD 157857, which we found to be possibly due to a nitrogen abundance lower than solar in HD 93843 (§ 4).

When we compare the giants to the supergiant stars discussed previously, the largest differences are the much weaker Si IV and S IV features, which almost disappear as P Cygni signatures at luminosity class III.

Another very conspicuous change is a weaker C III λ1175 + C IV λ1169: in the giants the absorption from this complex blend reaches a depth of about 40% of the continuum level, while in the two top supergiants the absorption is almost saturated. From this comparison, the differences between HD 210839 and the other supergiants appears to have a plausible explanation that HD 210839 is of intermediate luminosity class between supergiants and giants. In fact, C III λ1175 + C IV λ1169, as well as S IV and Si IV, are intermediate between the rest of the supergiant sample and our giant sample. Therefore, we revise the classification of its luminosity class to II. The only feature inconsistent with this picture is the C IV emission, which is stronger in HD 210839 than in any other star of the sample and may support its "f" designation. Underhill (1995) also suspected that HD 210839 could be of a luminosity class intermediate between supergiant and giant, based on the amount of Stark broadening of the He II lines in the optical spectra. Independently of the morphological classification, we do find from the model analysis that the star has a smaller radius than the other supergiants (Table 2) and a slightly higher $T_{\rm eff}$, consistent with its earlier subtype, than the other supergiants.

O VI is again a strong P Cygni profile in the giant stars, not appreciably different from in the supergiants.

3.3. *The O6 Dwarf*

For all the lines discussed above, we note a continuous trend from the top to the bottom of our plots. Notably, the N IV, Si IV, C III, P V, and S IV decrease drastically in the spectra of HD 101298, which has the lowest luminosity in our sample. As shown by our model analysis in the following sections, these changes are not just due to differences in luminosity (or temperature) but to variations of mass-loss rates and shocks across the luminosity classes.

Overall, the lines vary smoothly in the comparative plots (Figs. 1 and 2) given the sequence in which the stars have been arranged, supporting the suggestion that HD 210839 has a luminosity intermediate between the supergiants and the giants.

4. QUANTITATIVE SPECTRAL MODELING

In order to derive the stellar parameters from a consistent, quantitative analysis of the spectral features, we computed synthetic model spectra with mass loss in the UV and far-UV range using the WM-BASIC code, version 1.22 (Pauldrach, Hoffmann, & Lennon 2001). The code computes the underlying atmosphere and the synthetic spectrum by solving the wind hydrodynamics with non-LTE line-blanketing treatment and includes the effects of sphericity and expansion. By modeling transitions in the whole 905–2000 Å range, we were able to obtain a unique solution for $T_{\rm eff}$, $\log g$, $\log(L_{\rm bol}/L_\odot)$, V_∞, $\dot{M}$, and shocks and a check on the stellar abundances. Soft-X rays produced by shocks in the wind affect the ionization of the main observed stages (to different extents) and were taken into account in the ionization calculations, since this was proven necessary to reproduce all the observed lines consistently. In particular, O VI $\lambda\lambda$1032, 1037 is entirely produced by X-ray ionization, in the range of parameters explored in this work. X-rays also significantly affect the relative strength of N V (and C IV) versus Si IV in the *IUE* range and—to a lesser extent—the strength of P V $\lambda\lambda$1118, 1128, which is one of the few nonsaturated lines and thus very sensitive to all wind parameters. The effect of soft X-ray ionization is parameterized by the quantity $\log(L_{\rm X}/L_{\rm bol})$, whose values are found by varying this quantity as an additional free parameter in fitting the observed spectra (Table 2). Soft X-rays contribute to the ionization both by photoionization and by Auger ionization. The version of WM-BASIC that we used includes both processes (Pauldrach et al. 2001). Existing X-ray flux measurements for our objects are reported in Table 1 for

TABLE 2
STELLAR PARAMETERS FROM MODEL FITTING

Star	$T_{\rm eff}$ (10^3 K)	$\log g$	$R/R_\odot$	V_∞ (km s^{-1})	$\dot{M}$ ($M_\odot$ yr^{-1})	$\log(L_{\rm bol}/L_\odot)$	$\log(L_{\rm X}/L_{\rm bol})$	$\log L_{\rm X}$ (ergs s^{-1})
HD 163758.....	32^{+2}_{-1}	3.4 ± 0.2	21 ± 2	2100 ± 200	$(5.0 \pm 3.0) \times 10^{-6}$	$5.6^{+0.2}_{-0.1}$	-6.50 ± 0.20	32.7
HD 192639.....	33 ± 2	3.4 ± 0.2	20 ± 2	2050 ± 200	$(2.0 \pm 1.0) \times 10^{-6}$	5.6 ± 0.2	-6.70 ± 0.20	32.5
HD 210839.....	34 ± 2	3.5 ± 0.1	18 ± 2	2100 ± 200	$(1.5 \pm 0.5) \times 10^{-6}$	5.6 ± 0.2	-6.75 ± 0.20	32.4
HD 157857.....	34 ± 2	3.6 ± 0.1	16 ± 2	2250 ± 150	$(1.2 \pm 0.4) \times 10^{-6}$	5.5 ± 0.2	-6.75 ± 0.25	32.3
HD 93843	34 ± 2	3.6 ± 0.1	16 ± 2	2400 ± 200	$(0.6 \pm 0.3) \times 10^{-6}$	5.5 ± 0.2	-6.85 ± 0.15	32.2
HD 101298.....	33^{+2}_{-1}	4.0 ± 0.1	9 ± 2	2900 ± 150	$(0.4 \pm 0.2) \times 10^{-7}$	4.9 ± 0.2	-7.40 ± 0.20	31.1

comparison with our value of $\log(L_X/L_{bol})$ determined by the spectral fit (Table 2). While the measured L_X in Table 1 is the radiation escaping the star, $\log(L_X/L_{bol})$ determined by the spectral fit reflects the (soft) X-rays absorbed within the stellar envelope. The comparison gives some insight into the geometry of the shock region (§ 5).

From a vast set of model calculations, we determined the best fit to the observed spectra and constrained the uncertainty range of each parameter. This procedure required a much larger set of models than just varying the effective temperature and adopting reasonable values for the other parameters, but provided a check for the validity and the uniqueness of our solutions as well. In fact, variations of different parameters can compensate each other's effect on the line profiles, but when all lines are taken into account, a unique solution can be determined. Results from model fits are given in Table 2. Below we comment on the major effects of various parameters on the synthetic model spectra and the criteria that led to the adopted solutions for the individual stars. The discussion is somewhat lengthy; however, this is the first attempt to actually fit *all* observed far-UV and UV features, and we think our process provides some interesting insights.

4.1. *HD 210839*

We begin with HD 210839 because it has been extensively analyzed in the optical range. Herrero, Puls, & Villamariz (2000) derived $T_{eff} = 41,500$ K from plane-parallel, hydrostatic model analysis of optical spectra and $T_{eff} = 37,000$ K [$\log g = 3.55$, $\dot{M} = 6 \times 10^{-6}\ M_\odot\ yr^{-1}$, $\log(L_{bol}/L_\odot) = 5.78$] by analyzing the same data with spherical models including mass loss. Puls et al. (1996) derived for the same star $T_{eff} = 38,000$ K, $\dot{M} = 5 \times 10^{-6}\ M_\odot\ yr^{-1}$, $\log g = 3.65$, $\log(L_{bol}/L_\odot) = 5.83$, from the analysis of the Hα and Hγ lines.

Therefore, we started our analysis with a grid of models around these values and varied other parameters maintaining these temperatures.

Figure 3 shows that a model computed with the parameters from Herrero et al. (2000; models with sphericity) can reproduce only a few features (notably C IV in the *IUE* range, which is, however, saturated and thus less sensitive to the main parameters, as will be shown again later) but fails to reproduce the Si IV profile. Additionally, N V is too weak in the model and O VI is absent, while P V and C III λ1175 are almost saturated in the model. One parameter to which the optical line analysis is insensitive is the amount of X-rays (from shocks) contributing to the ionization, which essentially affects the higher ionization species, seen most notably in the UV and far-UV. Thus, we varied this parameter first, maintaining the high mass-loss rate and the temperature from the Herrero et al. analysis. The fits of the P V, C III λ1175, and N V λ1240 transitions are improved by adding the effect of shocks in the model, with $\log(L_X/L_{bol}) = -7.0$, but Si IV almost disappears in the model spectra with shocks. Also, decreasing the mass-loss rate further improves the match to P V and N V but worsens the match to Si IV and C IV. These effects are shown in the upper panel in Figure 3. We similarly tested other parameter changes and their extensive combinations, but no solution could be found that could match all the observed lines at $T_{eff} = 37,000$ K or higher.

We proceeded by lowering the temperature in small steps (500–1000 K) and varying all possible wind parameters [primarily mass-loss rate, V_∞, $\log(L_X/L_{bol})$, as well as secondary parameters such as the velocity law] at each T_{eff} value. Different values of gravity and luminosity were also investigated for all combinations.

At $T_{eff} = 36,000$ K, again the Si IV feature is produced only for very high mass-loss rates (a few $\times\ 10^6\ M_\odot\ yr^{-1}$), for a sensible range of gravity values ($\log g = 3.2$–3.6), in absence of X-ray ionization. But for reasonable values of shocks [$\log(L_X/L_{bol}) \approx -7.0$], which improve the match to other lines in the *FUSE* range, the Si IV line can be reproduced only with mass-loss rates of the order of $10^5\ M_\odot\ yr^{-1}$. However, no combination of parameters can provide an acceptable fit to the other lines in the *FUSE* range (in particular, O VI and P V) for such high $\dot{M}$ values. The best compromise match to all the features at $T_{eff} = 36,000$ K is reached for $\dot{M} \approx 4 \times 10^{-6}$ and $\log(L_X/L_{bol})$ between -6.7 and -7.0, the first yielding a better fit to P V and the second to O VI. In all models, Si IV and C III are not well reproduced.

A better match to all lines is achieved for a model at $T_{eff} = 35,000$ K, with $\dot{M} = 1.5 \times 10^{-6}\ M_\odot\ yr^{-1}$, $\log(L_X/L_{bol}) = -6.7$, $\log(L_{bol}/L_\odot) = 5.53$, and $\log g = 3.6$. Therefore, we adopt $T_{eff} = 35,000$ K as an upper limit to a range of acceptable fits.

At $T_{eff} = 34,000$ K, we find the best fit, shown in Figure 3 (*middle plot, lower panels*), for $\dot{M} = 1.7 \times 10^{-6}\ M_\odot\ yr^{-1}$, $\log(L_X/L_{bol}) = -6.75$, $\log(L_{bol}/L_\odot) = 5.6$, $R = 18 \pm 2\ R_\odot$, and $\log g = 3.5 \pm 0.1$. Si IV is slightly underestimated in this model, and it is best reproduced with $\dot{M} = 2 \times 10^{-6}\ M_\odot\ yr^{-1}$ and/or with a lower radius ($R = 16\ R_\odot$), whereas other lines are slightly overestimated in the models with these latter parameters. These comparisons define the adopted uncertainties.

For lower temperatures, at $T_{eff} = 33,000$ K, the influence of the parameters on most features is similar to what seen in the grid of models at $T_{eff} = 34,000$ K; however, for similar parameter combinations, cooler lines such as C III and Si IV (and to a lesser extent P V) are enhanced relative to the hotter lines of N V and C IV. The relative line strengths can be matched at the lower T_{eff} values by increasing the amount of shocks, which favors higher ions. Two interesting facts emerged. First, the dependence of the spectral lines on stellar luminosity and radius is the same at $T_{eff} = 34,000$ K and $T_{eff} = 33,000$ K, confirming that these parameters can be well constrained independently of other factors. Second, for given values of $\log(L_X/L_{bol})$, the strength of O VI at both $T_{eff} = 34,000$ K and $T_{eff} = 33,000$ K varies drastically in the same way, with stellar luminosity and with the mass-loss rate. In particular, once we fix the amount of shocks to $\log(L_X/L_{bol}) = -6.75$ and $\dot{M} = $ a few $\times\ 10^{-6}\ M_\odot\ yr^{-1}$ from other line ratios as explained above, O VI is almost absent in models with $\log(L_{bol}/L_\odot) \leq 5.5$ and $R = 16\ R_\odot$ and becomes saturated at $\log(L_{bol}/L_\odot) = 5.8$ and $R = 22\ R_\odot$. For $\dot{M} \geq 4 \times 10^{-6}\ M_\odot\ yr^{-1}$, the effect disappears, and O VI cannot be reproduced as a P Cygni profile. Therefore, once other parameters are constrained by the relative ratios of several other features, with their combination slightly varying with temperatures, O VI additionally constrains the stellar luminosity and mass-loss rate rather independently of temperature (between 34,000 K and 33,000 K). This line seems to have a "hard threshold" within these narrow ranges of stellar parameters. It requires a certain amount of

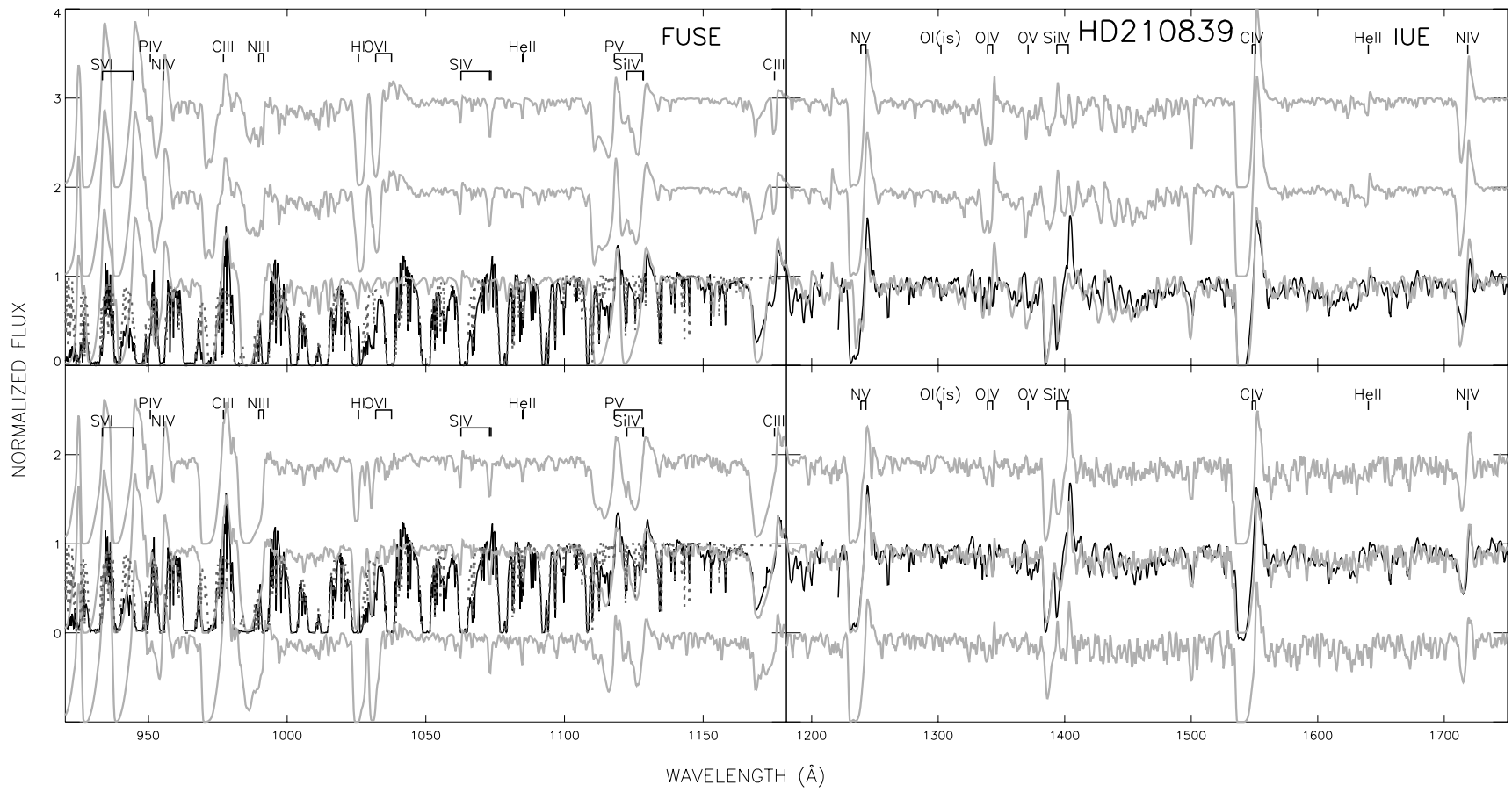

FIG. 3.—Model fits for HD 210839 (*FUSE* and *IUE* ranges in left and right panels, respectively; black lines are the observed spectra). *Upper panels*: WM-BASIC model (*gray thick line*) calculated with parameters from a recent study in the optical range by Herrero et al. (2000): $T_{\rm eff} = 37,000$ K, $\log g = 3.55$, $\dot{M} = 6 \times 10^{-6}\ M_{\odot}\ {\rm yr}^{-1}$, and $\log(L_{\rm bol}/L_{\odot}) = 5.78$. The optical analysis neglects the shocks in the wind, thus underestimating high ionization stages, especially O VI (*FUSE* range) and N V (*IUE* range). For the same reason, low-ionization species such as C III and P V are severely overestimated by the model. The middle plot in the stack was computed with the same stellar parameters as derived by Herrero et al., but adding the effect of shocks [$\log(L_{\rm X}/L_{\rm bol}) = -7.0$], which improves the match to the lines of N V and O VI; the model lacks Si IV and C III though, while P V is still in excess. Decreasing $\dot{M}$ to $4 \times 10^{-6}\ M_{\odot}\ {\rm yr}^{-1}$ (*upper plot*) reduces the strength of P V but also of Si IV, thus not solving the mismatch. No good fit could be found at $T_{\rm eff} = 37,000$ K or higher. *Lower panels*: Best-fit model [$T_{\rm eff} = 34,000$ K, $\log g = 3.5$, $\dot{M} = 1.7 \times 10^{-6}\ M_{\odot}\ {\rm yr}^{-1}$, $\log(L_{\rm bol}/L_{\odot}) = 5.6$, and $\log(L_{\rm X}/L_{\rm bol}) = -6.75$] is shown over the spectrum (*middle plot*). The other two models differ only in gravity and luminosity, having $\log g = 3.4$, $\log(L_{\rm bol}/L_{\odot}) = 5.8$ (*lower plot*) and $\log g = 3.6$, $\log(L_{\rm bol}/L_{\odot}) = 5.5$ (*uppermost plot*). These are shown to illustrate how sensitive the process is to the combination of multiple parameters and as an example of the fine grid of models that was computed around the best-fit parameters to determine uncertainties. [*See the electronic edition of the Journal for a color version of this figure.*]

X-rays to be produced at all, but then it also constrains $\log(L_{bol}/L_{\odot})$ and $\dot{M}$. A hard threshold for the onset of O VI as a P Cygni profile was also noted by Walborn et al. (2002) in a comparative *FUSE* spectral atlas.

At $T_{eff} = 32,000$ K, the parameters of the best fits found at higher temperatures produce models with much weaker N V, slightly weaker C IV, and much stronger C III. To maintain relative line strengths that match the observed spectrum, higher $\log(L_X/L_{bol})$ values are required at the lower temperature. However, the C III multiplet remains saturated in the models even at $\log(L_X/L_{bol}) = -6.3$ for $\dot{M}$ larger than $\approx 10^{-6}$ $M_{\odot}$ yr^{-1}. The C III observed strength requires $\dot{M} \leq 6 \times 10^{-7}$ $M_{\odot}$ yr^{-1} in the $T_{eff} = 32,000$ K models, which, however, causes other lines, most notably Si IV and N IV, to be too weak. In summary, it becomes impossible to reproduce consistently the lines, especially because of the strong change (decrease) of N V in the models when T_{eff} decreases below 33,000 K. Therefore, this value can be considered a conservative lower limit to the range of acceptable temperatures.

The best-fit model for HD 210839 is shown in Figure 3 with other models to illustrate the sensitivity to the parameters described above.

Although the requirement to match all far-UV and UV lines constrains the T_{eff} values between 33,000 and 35,000 K, we adopted in Table 2 an error twice as large, to allow for possible (and unquantifiable at this stage) limitations of the model calculations, although other works have found basically consistent results between WM-BASIC calculations and calculations with, e.g., CMFGEN (Hillier & Miller 1998). We will return to this point in the last section (§ 5). We adopt this criterion in estimating the errors for all stars analyzed.

4.2. *HD 163758 and HD 192639*

For these two supergiants we followed the same procedure as above. As noted in § 3, the main differences with respect to HD 210839 are the much stronger P Cygni profiles of C III λ1175 and Si IV, which suggest lower T_{eff} values and/or higher mass-loss rates. In fact, we find that the best overall fits to all spectral features can be achieved for a temperature of $T_{eff} = 32,000$ K for HD 163758 (and a mass-loss rate of $\dot{M} = 5 \times 10^{-6}$ $M_{\odot}$ yr^{-1}, a factor of 2 higher than for HD 210839) and $T_{eff} = 33,000$ K for HD 192639. In the fit of HD 163758, a small mismatch remains in the O VI doublet (underestimated) and the P V doublet (overestimated). These features are perfectly matched by models with $\dot{M} = 2 \times 10^{-6}$ $M_{\odot}$ yr^{-1} and an even higher $\log(L_X/L_{bol}) = -6.3$. This change of parameters, however, degrades the fit to other lines. Therefore, we adopt these ranges as the uncertainties in our parameter determinations. The T_{eff} values slightly lower than our value for HD 210839 are consistent with their later spectral subtypes.

One criterion to choose between $T_{eff} = 32,000$ K and $T_{eff} = 33,000$ K, additional to the overall relative line strengths, which are easier to reproduce in one case or the other, was the shape of the N V emission (Fig. 4). A weak, photospheric absorption of C III λ1247 appears at $T_{eff} = 32,000$ K, causing a small dip in the N V emission and increasingly suppressing it at lower temperatures. This dip is seen in the spectrum of HD 163758 but not in the N V profile of HD 192639. The difference is also seen in their respective best-fit models (Fig. 4).

We show an additional model besides the best-fit model to HD 192639, to illustrate the effect of changing the nitrogen abundance: lowering the abundance by a factor of 10 with respect to solar, the N IV lines vary significantly, while the saturated N V absorption shows no effect. Thus, the variations seen in the N V strength among these two stars are not due to abundance variations but to the small temperature difference.

4.3. *HD 93843 and HD 157857*

For HD 93843 we again tried a very extensive number of parameter combinations, for T_{eff} varying in small steps. For this object, we show (Fig. 5) a model that provides an excellent fit to all lines *except* the O VI doublet, especially to the lines in the *IUE* range. This model, with $T_{eff} = 34,000$ K and very low X-rays, is included in the figure as an example of the unique information provided by the *FUSE* range to constrain all stellar parameters consistently: this model matches perfectly the *IUE* spectrum and could have been adopted as a solution if the information from the *FUSE* spectrum were not available, further constraining the parameters. The O VI P Cygni profile can be reproduced only with a higher X-ray contribution to the ionization, as shown in the top plots of Figure 5. However, all models that can match both O VI and the cooler lines predict a N V feature stronger than the observed one. An overall good fit was achieved by lowering the nitrogen abundance by a factor of 10 with respect to solar values (Fig. 5, *top model*). Again, the uncertainties were estimated by computing a large set of models with parameters varying about the adopted solution.

Acceptable fits are again obtained for T_{eff} values between 36,000 and 32,000 K. At $T_{eff} = 37,000$ K, the strong lines in the *IUE* range (C IV and N V) can still somehow be reproduced for certain values of mass loss (between 10^{-6} and 10^{-7} $M_{\odot}$ yr^{-1}) and a low $\log(L_X/L_{bol})$ (-8.3), but the observed Si IV, P V, and O VI lines cannot be matched with the same parameters.

The other giant star of our sample, HD 157857, has a stronger Si IV doublet, which can be explained with a lower temperature and/or a higher mass-loss rate. We find that a lower temperature does not produce good fits to the other features, while a higher (by a factor of 2) mass-loss rate yields the best fit, for models in a temperature range between $T_{eff} = 34,000$ and 35,000 K (Fig. 5).

4.4. *HD 101298*

After calculating numerous models varying T_{eff}, $\log g$, $\log(L_{bol}/L_{\odot})$, $\dot{M}$, R, V_{∞}, and $\log(L_X/L_{bol})$, similar to the previous cases, we obtained an excellent fit of all features in the whole *FUSE*+*IUE* range (Fig. 6). The match to *all* the far-UV and UV lines by the model spectrum in this case is of unprecedented quality, as far as we know. Again, this result required a much wider grid of models and parameter combinations than is usually calculated in similar works. We invested such an enormous effort in this case in order to assess whether the code used is adequate for treating the different layers of the stellar envelope probed by our wide range of transitions, or whether the approximate or partial fits usually achieved in previous and similar works are an intrinsic limitation of the model assumptions. Although such a lengthy analysis would be impractical for a large number of stars, it is encouraging that in this case *all* lines

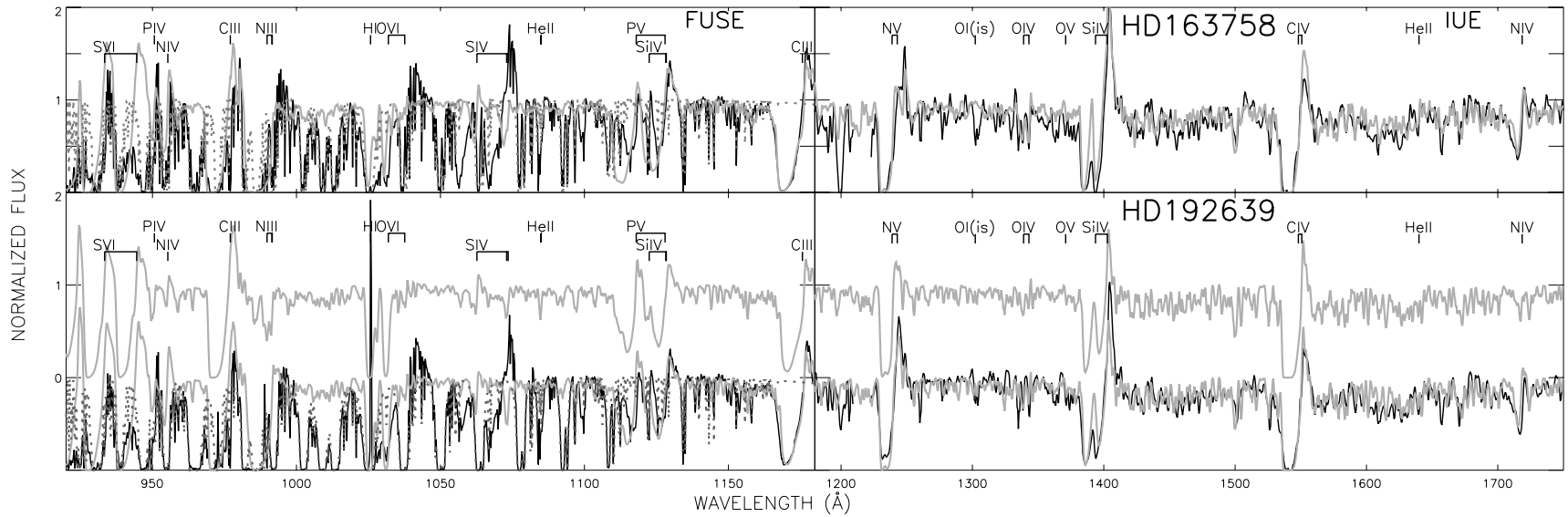

FIG. 4.—Model fits for the other two supergiant stars of our sample. *Upper panels*: HD 163758. *FUSE* and *IUE* spectra (*black line*) and best-fit model (*gray thick line*) with $T_{\rm eff} = 32,000$ K, $\log g = 3.4$, $\dot{M} = 5 \times 10^{-6}\ M_{\odot}\ {\rm yr}^{-1}$, $\log(L_{\rm bol}/L_{\odot}) = 5.6$, and $\log(L_{\rm X}/L_{\rm bol}) = -6.5$. *Bottom panels*: HD 192639. The best-fit model is overplotted [$T_{\rm eff} = 33,000$ K, $\log g = 3.4$, $R = 20\ R_{\odot}$, $\dot{M} = 2 \times 10^{-6}\ M_{\odot}\ {\rm yr}^{-1}$, $\log(L_{\rm bol}/L_{\odot}) = 5.6$, and $\log(L_{\rm X}/L_{\rm bol}) = -6.7$]. The same model but with a nitrogen abundance of 0.1 solar is plotted with an offset. N V is not affected (because saturated), but the N IV line almost disappears. [*See the electronic edition of the Journal for a color version of this figure.*]

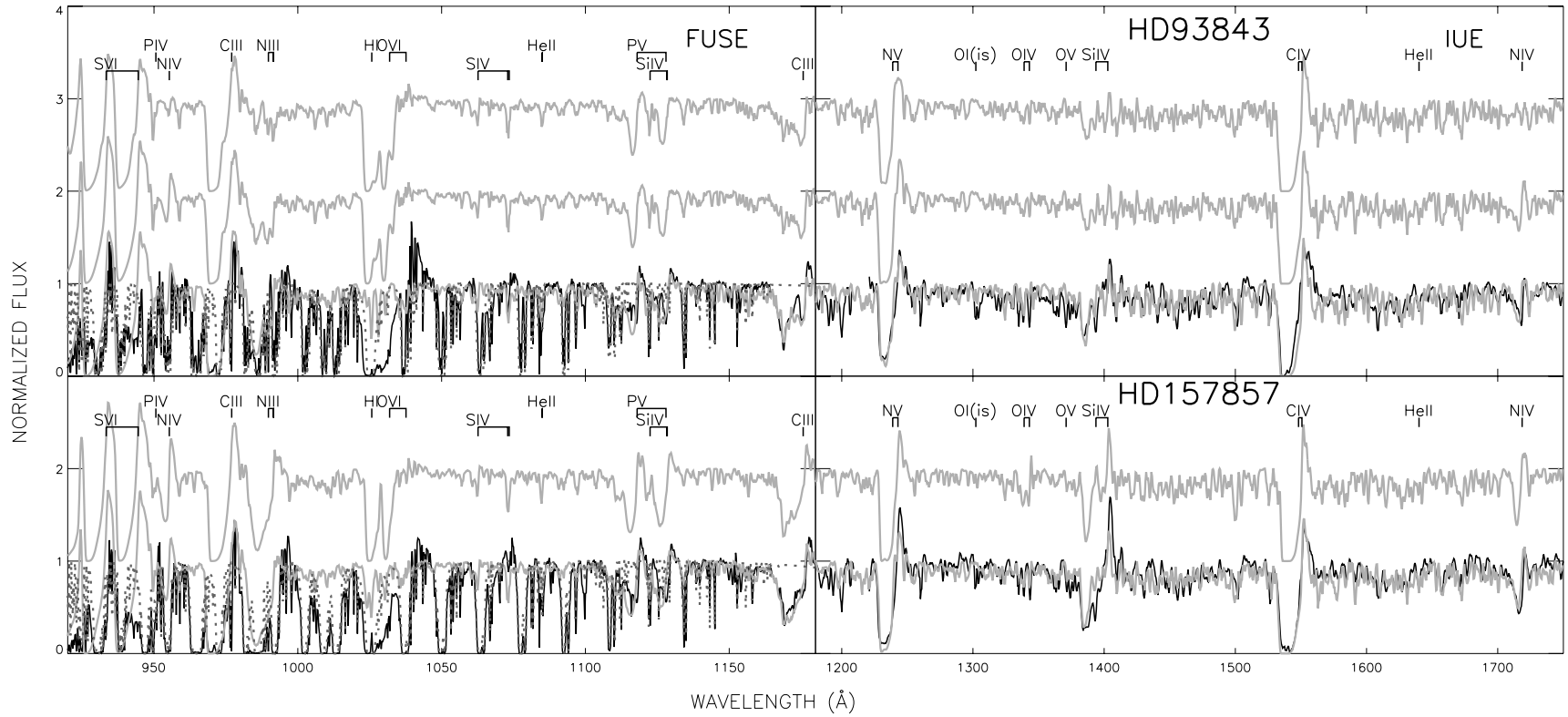

FIG. 5.—Model fits for the giant stars (symbols as in previous figures). *Upper panels*: HD 93843. The model overplotted to the spectrum has $T_{\rm eff} = 34,000$ K, $\log g = 3.6$, $R = 16\ R_\odot$, $\dot{M} = 6 \times 10^{-7}\ M_\odot\ {\rm yr}^{-1}$, $\log(L_{\rm bol}/L_\odot) = 5.5$, and $\log(L_{\rm X}/L_{\rm bol}) = -7.5$. It provides an excellent fit to all lines except for underestimating the O VI line; this line is reproduced by higher shocks [*middle plot*; $\log(L_{\rm X}/L_{\rm bol}) = -6.85$], although the line of N V is now too strong. The mismatch is solved by lowering the abundance of nitrogen to 0.1 the solar value (*upper plot*). *Lower panels*: HD 157857. Two models are shown, with $T_{\rm eff} = 34,000$ K (*lower plot*) and $T_{\rm eff} = 35,000$ K (*upper plot*). Both have $\log g = 3.6$ and $\log(L_{\rm bol}/L_\odot) = 5.5$. However, the lower model has $\dot{M} = 8.5 \times 10^{-7}\ M_\odot\ {\rm yr}^{-1}$ and $\log(L_{\rm X}/L_{\rm bol}) = -7.0$ (the O VI line is underestimated), and the upper model has $\dot{M} = 1.6 \times 10^{-6}\ M_\odot\ {\rm yr}^{-1}$ and $\log(L_{\rm X}/L_{\rm bol}) = -6.5$, which provide the best match to the O VI doublet but slightly overestimate N V. These provide another example of how the uncertainties have been determined. [*See the electronic edition of the Journal for a color version of this figure.*]

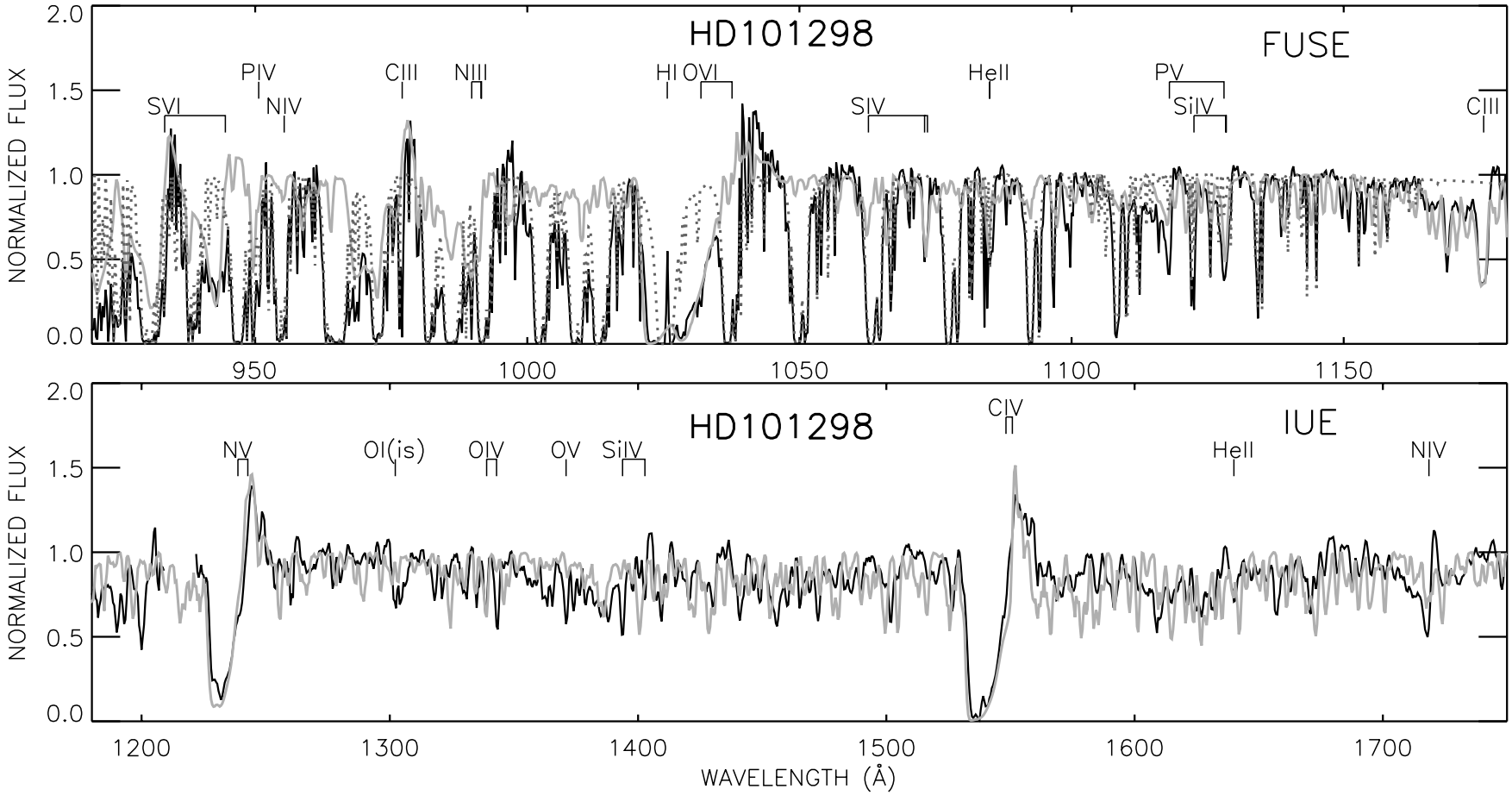

FIG. 6.—Spectra of HD 101298 and best-fit model (colors/lines as in previous plots; parameter ranges constrained by the acceptable models given in Table 2). Note an excellent match to the O VI line as well as to all lines in the *IUE* range and to the various sulfur ionization stages, shown in detail in the next figure. [*See the electronic edition of the Journal for a color version of this figure.*]

corresponding to different temperatures, thus arising in different wind layers, could be modeled very well. The best-fit model is shown in Figure 6. Note that a large part of the O VI profile is not affected by the interstellar absorptions, and it is perfectly matched by the model. This line is very sensitive to $\log(L_X/L_{bol})$ and to the mass-loss rate. The S IV lines, much less conspicuous in this star than in the higher luminosity ones, were also crucial in determining the overall parameters (Fig. 7). The S IV components at $\lambda\lambda$1072.9, 1073.52 are well matched by the model (the component at λ1062.67 is buried in a strong H_2 absorption); see Figure 7. These transitions strongly vary with luminosity class, similarly to Si IV, because they are very sensitive to the mass-loss rate, as shown by the comparison among our sample spectra. This effect was noted by Walborn & Bohlin (1996) in the analysis of *Copernicus* data and can be now quantified thanks to spectral resolution of *FUSE*, which allows us to disentangle the interstellar lines from the stellar features. Although the resonance lines of S VI fall in a wavelength range heavily absorbed by the interstellar hydrogen (making flux normalization difficult), they are also well matched by our models. Note the match of the model to the spectra in the windows free of interstellar hydrogen absorptions: the emission of the blue component and the absorption trough of the red component (Fig. 7, *lower panel*).

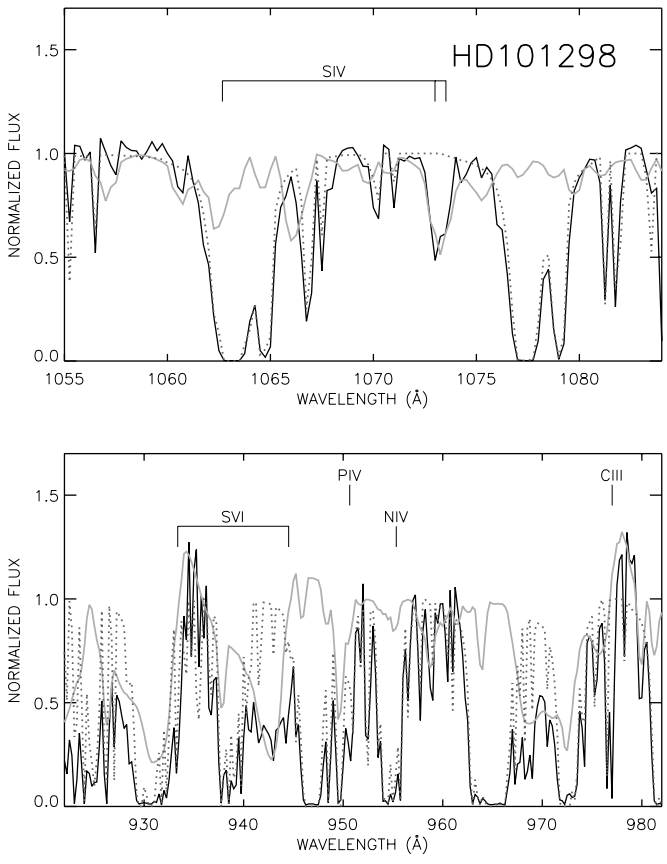

FIG. 7.—S IV multiplet and S VI doublet in the HD 101298 spectrum and best-fit model (same as in Fig. 6) shown on expanded scale. The bluer component of S IV is masked by interstellar absorption (*dotted line*). The rest-wavelength positions are marked. Note the excellent match to the red (uncontaminated) S IV component. As for S VI (*lower panel*), the absorption of the blue component and the emission of the red component are completely absorbed by ISM bands. However, note the good match of the model in the two windows free of ISM absorptions, i.e., the emission of the blue component and the depth of the absorption in the red component. This figure shows the unique capability afforded by the *FUSE* range to constrain the hitherto elusive ionization in the hot star winds. Other nearby lines show the complexity of analyzing this spectral region. [*See the electronic edition of the Journal for a color version of this figure.*]

4.5. *The Sulfur Ionization*

In all models computed in the T_{eff} range of our sample, we achieved an unprecedentedly good fit of all wind and photospheric lines, except for the P Cygni profile of S IV in the *supergiant stars*, where this line is seen as a conspicuous P Cygni profile (with an absorption decreasing from almost saturated in HD 163758 to 50% in HD 192639 to about 70% of the continuum intensity in HD 210839). Note instead that S IV is perfectly matched by the model spectra in the dwarf star of the sample (Fig. 7 and previous section). The S IV doublet begins to appear in our models for supergiants as a small P Cygni profile (depth of the absorption about 70% of the continuum, when we degrade the model resolution to 0.25 Å bins, for comparison with our *FUSE* spectra) at $T_{eff} \approx 34,000$ K for $\dot{M} = 6 \times 10^{-6}$ $M_\odot$ yr^{-1} or at $T_{eff} \approx 33,000$ K for $\dot{M} = 2 \times 10^{-6}$ $M_\odot$ yr^{-1} [with $\log(L_X/L_{bol}) = -7$]. Its intensity increases with higher mass-loss rates and with decreasing shocks and temperature. For $\dot{M} = 6 \times 10^{-6}$ $M_\odot$ yr^{-1} [$\log(L_X/L_{bol}) = -7$], the models predict a fully developed S IV P Cygni profile of strength similar to the observed one only at T_{eff} values as low as 26,000 K. Since our derived mass-loss rates are generally lower than this value, an even lower temperature would be required to fit this line, inconsistent with the rest of the spectrum.

The hotter S VI doublet at 933 and 944 Å is seen as a fully developed P Cygni profile in all the spectra, although it lies in a spectral region highly affected by ISM absorption, and it is similarly predicted by the models.

According to our model calculations, there are two S V lines at 1199 and 1500 Å. However, nearby lines from other ions complicate their analysis; especially, the line at ≈1200 Å is mostly due to Si III transitions. This feature is predicted by our models to increase with increasing mass loss and with decreasing T_{eff} values and shocks, a behavior similar to Si IV and S IV, for supergiants. A group of Si III lines (multiplet 36) is also present between 1500.2 and 1501.9 Å. In the figures showing our best-fit models for the supergiants, the observed λ1500 line is well matched for all stars.

We plan to investigate in subsequent work whether the problem in reproducing the S IV lines in the spectra of the high-luminosity stars is due to some assumptions in the WM-BASIC code. Because the observed S IV, S V, and S VI lines in our dwarf star are instead extremely well matched by the models (Fig. 7), we suspect that the temperature and density structure of the wind in the outer layers of the extended envelopes (for objects of high luminosity) is more complex than currently treated. This hypothesis is also supported by the shape of the O VI P Cygni profile in the model calculations: a fully developed P Cygni profile, perfectly consistent with the observed one, is achieved for models at low luminosities (Fig. 6), while in all high-luminosity models, this doublet remains narrower than the observed one. This limitation will be investigated in a separate paper.

Although we have no firm explanation at this point for the presence of the S IV P Cygni profile in the spectra of supergiants, calculations with the current WM-BASIC code point toward even lower T_{eff} values from this line than our

adopted solutions. The main result of the present analysis is significantly lower $T_{\rm eff}$ values than previously assumed for these spectral types; thus, the mismatch of the S IV line in the supergiants does not contradict this general finding.

5. DISCUSSION AND CONCLUSIONS

In this paper we have derived wind and photospheric parameters for a sample of mid-O stars covering a range of luminosity classes, by modeling their observed UV and far-UV spectra with the WM-BASIC code. We achieved model fits to the observed spectra of all wind and photospheric lines with better accuracy than previous partial analyses, thanks to a thorough investigation of the effects of all parameters. There are two main results.

First, the inclusion of certain ions observed only in the *FUSE* wavelength range (e.g., high-ionization species, such as O VI, and nonsaturated, non-CNO lines such as P V) in the analysis allows us for the first time to constrain all parameters consistently and therefore to dismiss solutions that would be acceptable based on the saturated CNO lines in the *IUE*/*HST* range alone (e.g., § 4.3) or in the optical range. A main advantage is the presence of the O VI doublet. Its ratio to other lines can uniquely be explained by the inclusion of soft X-rays in the wind ionization calculations. The main wind lines observed in the *IUE* range (N V, Si IV, and C IV) are mostly saturated, thus quite insensitive to a large range of parameters. Their relative strengths are also affected by the amount of soft X-rays; however, they can be reproduced by models neglecting X-rays in some cases by adjusting temperature and mass-loss rate. When the amount of X-rays is instead constrained by the inclusion of hotter lines in the *FUSE* range, a higher ionization is produced than in models without X-rays; therefore, the solution is uniquely constrained and yields lower temperatures.

Second, the effective temperatures derived for all stars in our sample are significantly lower than values previously believed typical for O6–O7 types and than most determinations from previous analyses of the same stars (see below). This finding has many important implications. The temperature ranges that we derived by modeling the UV and far-UV spectra of the O6 stars, $T_{\rm eff} = 32,000$–$34,000$ K, are significantly lower than canonical values attributed to their spectral type by empirical calibrations over the last decades. Vacca, Garmany, & Shull (1996) derived a $T_{\rm eff}$ calibration of O-type stars compiling determinations based on plane-parallel, non-LTE, pure H and He hydrostatic models. Their calibration gives $T_{\rm eff} = 41,710$, 42,640, and 43,560 K for O6 Ia, III, and V types, respectively. De Jager & Nieuwenhuijzen's (1987) calibration gives $T_{\rm eff} = 38,200$–$39,500$ K and 36,060–35,700 K from O6 and O7 supergiants (Ia+) to dwarfs—less discrepant, but still significantly higher than our findings. The comparison between our resulting $T_{\rm eff}$ values and these previous compilations is shown in Figure 8. Considering the uncertainties, the difference is rather independent of luminosity class. The luminosities derived from our analysis are also lower than the previous calibrations, and the comparison is given in the lower panel of Figure 8. We will separately analyze optical spectra for our program stars, to further investigate the cause of the discrepancy. While it is currently being recognized that the use of models with full line-blanketing treatment and sphericity in the optical range yields $T_{\rm eff}$ values lower than found by simplified (pure H and He) treatments, we also find in some cases

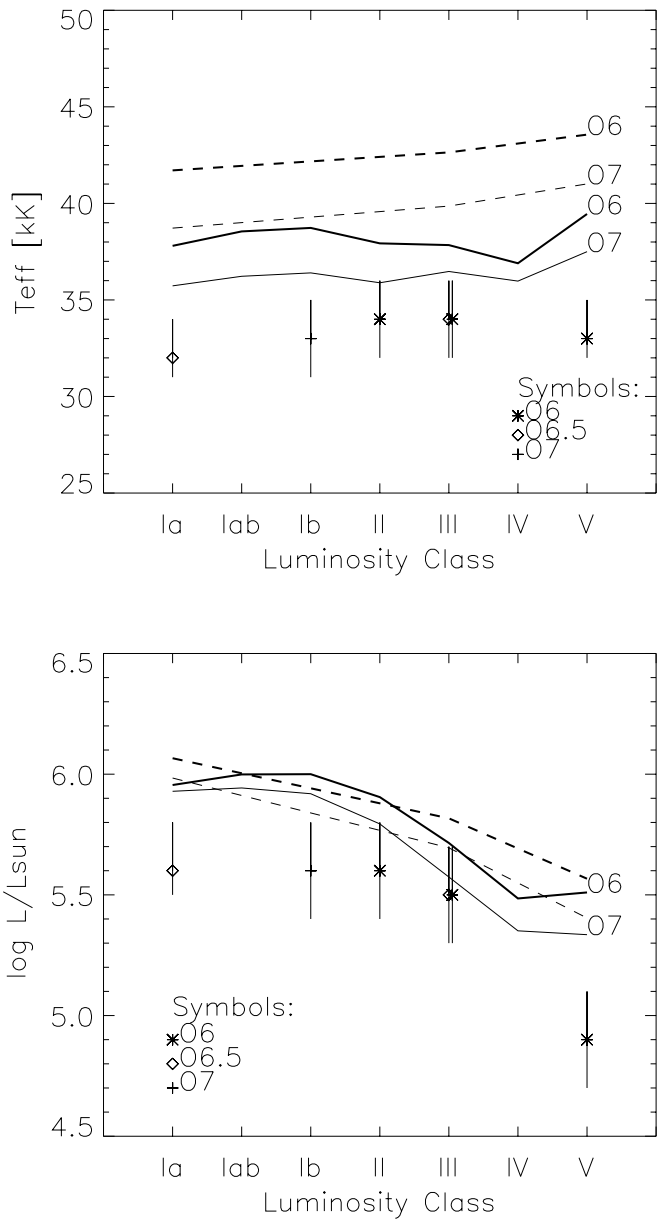

FIG. 8.—Effective temperatures and luminosities derived in this paper for the program stars (different symbols for spectral type subclasses) are compared to previous calibrations of $T_{\rm eff}$ and $\log(L_{\rm bol}/L_{\odot})$ vs. luminosity class for spectral types O 6 (*thick lines*) and O 7 (*thin lines*). The calibrations are from Vacca et al. (1996; *dashed lines*) and from de Jager & Nieuwenhuijzen (1987; *solid lines*). The differences from our results are rather independent of luminosity class, considering the uncertainties.

that the values of $T_{\rm eff}$ and $\log g$ derived in previous works can still somehow reproduce the lines in the *IUE* range (by neglecting X-ray ionization and other effects) but cannot reproduce all the lines observed in the *FUSE* range with the same combination of parameters. Crowther et al. (2002) analyze optical spectra of Magellanic Cloud O-type supergiants and extrapolate the results to the far-UV and UV, to test the robustness of the optical-line–based analysis. Significant discrepancies between their models and the observed spectra are seen in the far-UV to UV range.

The question remains open whether an accurate modeling of the optical spectra alone could provide similar results. Martins, Schaerer, & Hillier (2002) show that the inclusion

of line blanketing in model calculations yields $T_{\rm eff}$ values lower than analyses with pure H and He models. Herrero et al. (2000) demonstrated that inclusion of sphericity and mass loss in modeling optical data improves the results and yields lower temperatures compared with plane-parallel, hydrostatic models. Using the calibration computed by Martins et al. (2002) for O-type dwarfs, the measured ratio of He I λ4471/He II λ4542 in our optical spectra (L. Bianchi & M. Garcia 2002, in preparation) of HD 101298 yields $T_{\rm eff} \approx 39,000$ K, still significantly discrepant with the present analysis. By comparison with Conti's (1973b) calibration based on Auer & Mihalas (1972) non-LTE models, our measured ratios of He I λ4471/He II λ4542 correspond to $T_{\rm eff} = 41,000$ K for HD 101298, $T_{\rm eff} = 42,000$ K for HD 93843, and $T_{\rm eff} = 38,000$ K for HD 210839. These values are quite discrepant with our results from the full analysis of the far-UV and UV spectra. Future work will include the analysis of optical spectra of the same stars and the extension to other O types.

Most previous analyses for our program stars found higher $T_{\rm eff}$ values than our work, while other parameters, such as the mass-loss rate, are sometimes not significantly discrepant. For HD 163758, Gómez & Niemela (1987) derive $\dot{M} = (2\text{–}8) \times 10^{-6}\ M_{\odot}\ {\rm yr}^{-1}$ from the analysis of the Hα and He II λ4686 profiles. Lamers et al. (1999) derive $\dot{M} = 6 \times 10^{-6}\ M_{\odot}\ {\rm yr}^{-1}$ for HD 163758 and $\dot{M} = 2 \times 10^{-6}\ M_{\odot}\ {\rm yr}^{-1}$ for HD 210839, in agreement with our findings. For HD 192639, Puls et al. (1996) derive, by analyzing optical hydrogen and helium lines and UV (*IUE*) lines with plane-parallel hydrostatic non-LTE models, $T_{\rm eff} = 38,500$ K, $\log g = 3.45$, $\log(L_{\rm bol}/L_{\odot}) = 5.88$, $R/R_{\odot} = 19.5$, $\dot{M} = 6 \times 10^{-6}\ M_{\odot}\ {\rm yr}^{-1}$, and $V_{\infty} = 2150\ {\rm km\ s}^{-1}$, similar to a previous analysis by Herrero et al. (1992) except for $\log g = 3.35$ in the earlier work. The temperature and luminosity are substantially higher than in our analysis, while some other parameters do not differ so significantly. As reported in § 4.1, for HD 210839, Herrero et al. (2000) derived $T_{\rm eff} = 41,500$ K and $T_{\rm eff} = 37,000$ K from two different analyses of the same optical spectra, and Puls et al. (1996) derived $T_{\rm eff} = 38,000$ K from the analysis of the Hα and Hγ lines, again quite discrepant with our findings. To HD 101298, Conti & Burnichon (1975) assign a $T_{\rm eff} = 39,800$ K based on its optical spectrum and using the calibration of the He I/He II line ratios with $T_{\rm eff}$ by Conti (1973a). We note that, if we were to match the lines in the *IUE* range only (N V and C IV) with higher $T_{\rm eff}$ models (37,000 K or higher), without including shocks (which would be inconsistent with the O VI and other lines in the *FUSE* range), we would find higher mass-loss rates, similar to many of the previous analyses.

Morossi & Crivellari (1980) analyzed optical spectra using Auer & Mihalas (1972) plane-parallel non-LTE models and found $T_{\rm eff} = 35,500 \pm 700$ K, $\log g = 3.59 \pm 0.11$ for HD 192639 and $T_{\rm eff} = 32,200 \pm 2000$ K, $\log g = 3.7 \pm 0.23$ for HD 157857. This is the only work that we found to give temperatures consistent with our results, within the errors. Other studies derived $T_{\rm eff}$ and $L_{\rm bol}$ from photometric colors and magnitudes, thus not providing a significant comparison, and generally find higher temperatures. None of the previous works include the lines in the far-UV range, and most are based only on optical-line diagnostics.

Our main result is that we derive significantly lower effective temperatures than previously found by most other works for mid-O stars. This result has enormous implications for our understanding of the ionization and energy balance of H II regions, as well as in the context of evolution of massive stars. The lower temperatures, and consequently lower luminosities (Fig. 8), imply that the stars are less massive (and/or older) than previously thought, by comparison with evolutionary calculations. Additionally, the result has implications for energy balance calculations of H II regions. The photons emitted below the Lyman limit, which are driving the ionization of the surrounding medium, can be inferred only by accurate $T_{\rm eff}$ determinations at longer wavelengths.

As a result of our analysis, we also reclassified HD 210839 as O6f II.

Finally, our consistent analysis of lines from different ionic species also provided a handle on the presence of shocks and the effect of soft X-rays on the wind ionization. This parameter can be constrained only when "hot" lines such as O VI are observed and analyzed consistently with cooler lines. We fitted each star independently and found the best-fit model for each spectrum using the criteria explained in § 4, and $\log(L_{\rm X}/L_{\rm bol})$ (Table 2, eighth col.) was determined as a free parameter (§ 4). In the last column of the table, we give the soft X-ray luminosity, converting $\log(L_{\rm X}/L_{\rm bol})$ with the $\log(L_{\rm bol}/L_{\odot})$ values from our analysis (seventh col.), for comparison with the measured X-ray fluxes reported in Table 1. The amount of soft X-rays necessary to explain the observed ionization (Table 2) appears to decrease smoothly with stellar radius/luminosity, in our sample. No similar trend is seen in the measured X-ray emissions (Table 1). Bianchi (1983) found that while there is a strong correlation between V_{∞} and $\log(L_{\rm bol}/L_{\odot})$, there is weak or no correlation between V_{∞} and $L_{\rm X}$, in a sample of supergiants observed with *Einstein* and *IUE*. Also, our determined X-ray flux is generally lower (but of the same order) as the measured one, consistent with the fact that only the soft X-rays contribute to the ionization of the observed species (e.g., Pauldrach et al. 2001). The fact that X-rays (shocks) have a smaller effect in ionizing the winds in stars of smaller radii, regardless of the amount of X-rays emitted by the star, relates to the density structure in the outflowing material (see variations of $\dot{M}$ in Table 2), which vary with gravity, as can be expected. Further investigations will be conducted on the wind structure using WM-BASIC and other codes for comparison.

We are very grateful to James Herald for carefully reading the manuscript and providing valuable comments, to John Hutchings, who provided constant encouragement for progress of this project within the *FUSE* "hot stars team" and useful comments on the manuscript, to Alex Fullerton for his valuable advice about many aspects of the *FUSE* data reduction, to the *FUSE* Science Team for providing access to the data, and to Adi Pauldrach for useful discussions about the WM-BASIC code. This work is based on data obtained by the NASA-CNES-CSA *FUSE* mission operated by The Johns Hopkins University. This work also made use of *IUE* data obtained from both the INES archive and MAST. Financial support has been provided in part by NASA grants NRA-99-01-LTSA-029, NAG5-8965, and NAS5-32985.

REFERENCES

Auer, L., & Mihalas, D. 1972, ApJS, 24, 193
Berghoefer, T. W., Schmidtt, J. H. M. M., & Cassinelli, J. P. 1996, A&AS, 118, 481
Bianchi, L. 1983, Adv. Space Res., 2(9), 293
Bianchi, L., & Bohlin, R. C. 1984, A&A, 134, 31
Bianchi, L., Lamers, H. J. G. L. M., Hutchings, J. B., Massey, P., Kudritzki, R., Herrero, A., & Lennon, D. J. 1994, A&A, 292, 213
Bianchi, L., Scuderi, S., Massey, P., & Romaniello, M. 2001, AJ, 121, 2020
Bianchi, L., et al. 2000, ApJ, 538, L57
Bohlin, R. C., Savage, B. D., & Drake, J. F. 1978, ApJ, 224, 132
Chlebowski, T., Harnden, F. R., Jr., & Sciortino, S. 1989, ApJ, 341, 427
Conti, P. S. 1973a, ApJ, 179, 161
———. 1973b, ApJ, 179, 181
Conti, P. S., & Burnichon, M. L. 1975, A&A, 38, 467
Conti, P. S., & Leep, E. M. 1974, ApJ, 193, 113
Conti, P. S., Leep, E. M., & Lorre, J. J. 1977, ApJ, 214, 759
Crowther, P. A., Hillier, D. J., Evans, C. J., Fullerton, A. W., de Marco, O., Pellerin, A., & Willis, A. J. 2002, ApJ, 579, 774
de Jager, C., & Nieuwenhuijzen, H. 1987, A&A, 177, 217
Evans, D. S. 1967, in IAU Symp. 30, Determination of Radial Velocities and Their Applications, ed. A. H. Batten & J. F. Heard (New York: Academic Press), 57
Garrison, R. F., Hiltner, W. A., & Schild, R. E. 1977, ApJS, 35, 111
Gómez, D. O., & Niemela, V. S. 1987, Rev. Mexicana Astron. Astrofis., 14, 293
Herrero, A., Kudritzki, R. P., Vilchez, J. M., Kunze, D., Butler, K., & Haser, S. 1992, A&A, 261, 209
Herrero, A., Puls, J., & Villamariz, M. R. 2000, A&A, 354, 193
Hillier, D. J., & Miller, D. L. 1998, ApJ, 496, 407
Lamers, H. J. G. L. M., Haser, S., de Koter, A., & Leitherer, C. 1999, ApJ, 516, 872
Leep, E. M. 1978, ApJ, 225, 165
Martins, F., Schaerer, D., & Hillier, J. 2002, A&A, 382, 999
Mason, B. D., Gies, D. R., Hartkopf, W. I., Bagnuolo, W. G., Jr., Brummelaar, T. T., & McAlister, H. A. 1998, AJ, 115, 821
Massey, P. 1998, in Stellar Astrophysics for the Local Group, ed. A. Aparicio, A. Herrero, & F. Sánchez (Cambridge: Cambridge Univ. Press), 95
Mathys, G. 1988, A&AS, 76, 427
———. 1989, A&AS, 81, 237
McConnell, D. J., & Bidelman, W. P. 1976, AJ, 81, 225
Moos, H. W., et al. 2000, ApJ, 538, L1
Morossi, C., & Crivellari, L. 1980, A&AS, 41, 299
Pauldrach, A. W. A., Hoffmann, T. L., & Lennon, M. 2001, A&A, 375, 161
Pellerin, A., et al. 2002, ApJS, 143, 159
Penny, L. R., Gies, D. R., & Bagnuolo, W. G., Jr. 1996, ApJ, 460, 906
Perryman, M. A. C., et al. 1997, A&A, 323, L49
Prinja, R., & Crowther, P. A. 1998, MNRAS, 300, 828
Puls, J., et al. 1996, A&A, 305, 171
Rachford, B. L., et al. 2002, ApJ, 577, 221
Sahnow, D., et al. 2000, ApJ, 538, L7
Scuderi, S., & Panagia, N. 1992, ApJ, 392, 201
Thackeray, A. D., Tritton, S. B., & Walker, E. N. 1973, MmRAS, 77, 199
Underhill, A. B. 1995, ApJS, 100, 461
Vacca, W. D., Garmany, C. D., & Shull, J. M. 1996, ApJ, 460, 914
Walborn, N. R. 1972, AJ, 77, 312
———. 1973, AJ, 78, 1067
Walborn, N. R., & Bohlin, R. C. 1996, PASP, 108, 477
Walborn, N. R., Fullerton, A. W., Crowther, P. A., Bianchi, L., Hutchings, J. B., Pellerin, A., Sonneborn, G., & Willis, A. J. 2002, ApJS, 141, 443
Walborn, N. R., & Nichols-Bohlin, J. 1987, PASP, 99, 40
Walborn, N. R., Nichols-Bohlin, J., & Panek, R. J. 1985, *International Ultraviolet Explorer* Atlas of O-Type Spectra from 1200 to 1900 Å (NASA RP-1155)
Walborn, N. R., & Panek, R. J. 1984, ApJ, 286, 718
Wamsteker, W., Skillen, I., Ponz, J. D., de la Fuente, A., Barylak, M., & Yurrita, I. 2000, Ap&SS, 273, 155